Lithography-based fabrication of nanopore arrays in freestanding SiN and graphene membranes

Verschueren, Daniel V.; Yang, Wayne; Dekker, Cees

DOI
10.1088/1361-6528/aaabce

Publication date
2018

Document Version
Accepted author manuscript

Published in
Nanotechnology

Lithography-based fabrication of nanopore arrays in freestanding SiN and graphene membranes

Daniel V Verschueren[†], *Wayne Yang*[†], *and Cees Dekker*[1*]

Department of Bionanoscience, Kavli Institute of Nanoscience, Delft University of Technology,

Van der Maasweg 9, 2629 HZ, Delft, The Netherlands

E-mail: c.dekker@tudelft.nl

Abstract

We report a simple and scalable technique for the fabrication of nanopore arrays on freestanding SiN and graphene membranes based on electron-beam lithography and reactive ion etching. By controlling the dose of the single-shot electron-beam exposure, circular nanopores of any size down to 16 nm in diameter can be fabricated in both materials at high accuracy and precision. We demonstrate the sensing capabilities of these nanopores by translocating dsDNA through pores fabricated using this method, and find signal-to-noise characteristics on par with TEM-drilled nanopores. This versatile lithography-based approach allows for the high-throughput manufacturing of nanopores and can in principle be used on any substrate, in particular membranes made out of transferable 2D materials.

Keywords: nanopore array, reactive ion etching, 2D materials, graphene nanopore, electron beam lithography

---

[1*] To whom correspondence should be addressed. [†] These authors contributed equally.

Introduction

Solid-state nanopores drilled in a thin membrane are unique tools that allow for label-free high-throughput single-molecule investigation of biomolecules such as DNA, proteins, and peptides chains[1]. Their robustness, versatility, and ease of integration in CMOS processing are paramount to the sustained interest this class of biosensors has received over the past 15 years[2]. The principle of interrogation for nanopore sensing derives elegance from its simplicity: a nanopore, typically drilled in a 20nm thick membrane, defines a nanoscale sensing volume through which biomolecules can be probed on passage, usually via an ionic-current readout[3]. More recently, nanopores in single-layer materials like graphene and MoS_2 have received a great deal of attention, as the two-dimensional (2D) nature of these materials drastically reduces the sensing volume and helps to enhance the signal[4, 5]. Both SiN and 2D nanopores have been used to provide insight into many complex biophysical phenomena, such as DNA-protein interactions[4-8], protein-protein interactions[9], and DNA polymer physics[10, 11]. However nanopore fabrication is typically slow and expensive, particularly in 2D materials, preventing large-scale use of solid-state nanopores in commercial applications, such as clinical sensors for the detection of biomolecules in diagnostics[12, 13].

Currently, there are several techniques for the production of nanopores. First and foremost is the use of the electron beam of a Transmission Electron Microscope (TEM)[14]. This technique provides sub-nanometer precise control over the pore's diameter, but is very low in throughput, especially for larger sized nanopores (>15 nm)[15], very expensive, and labor

intensive. A single nanopore takes at least 30 mins to be loaded into the TEM, aligned and sculpted to the desired size in a TEM by a trained operator. Furthermore, nanopores are notoriously hard to fabricate in 2D materials with conventional TEM drilling due to their sensitivity to carbon deposition and membrane damage[16]. Hence, the method lacks scalability and cost efficiency which are both required for commercialization. Fabrication using Helium Ion Microscope (HIM) is a promising, more high-throughput alternative for the fabrication of nanopores, but also requires access to expensive and delicate instrumentation[17, 18]. An alternative cost-effective technique is nanopore fabrication by controlled dielectric breakdown, where a nanopore is created by the timed termination of a large transmembrane voltage stress (~10V)[19,20]. However, the stochastic nature of the breakdown process does not provide control over the position of the nanopore[21]. Other techniques use ion bombardment and subsequent chemical[22, 23] or electrochemical wet etching[24]. Whereas these techniques can be used at high throughput, challenges remain in the timed termination of the wet etching[15] and the associated uniformity of the pore size.

Chemical dry etching or reactive ion etching (RIE) is a more promising alternative for high-throughput fabrication of large nanopores. In this widely used technique a pattern is predefined in a resist by electron-beam lithography (EBL), which is the standard technique used to define high-resolution structure in microfabrication, and is transferred into a substrate by plasma etching using reactive ions[25]. The directionality of the RIE process preserves the resolution obtained in the EBL pattern and allows for the resolution to be defined on a wafer

scale[25-28]. The chemical dry etching allows a range of substrates to be used as membrane material[26], notably including 2D materials that require a transfer step. To exploit the potential of this technique for transferable materials, the EBL patterning should be performed on a freestanding membrane. Furthermore, patterning on a thin membrane can improve resolution, because it eliminates electron backscatter [29].

Here, we present a novel and simple method for rapid nanopore fabrication based on electron-beam lithography with reactive ion etching. By patterning the nanopores as a last step in the fabrication process, in principle any (transferable) membrane material can be readily used. To demonstrate the flexibility of this technique, we create single nanopores and nanopore arrays in both 20 nm thick SiN and single-layer graphene membranes. TEM inspection shows that the fabricated nanopores are highly circular and uniform in size. We show that the nanopore diameter can be set with nanometer precision by controlling the electron-beam dose. Finally, we demonstrate lambda-DNA translocations through nanopores fabricated using this method. Although applied here for single-molecule biosensing, we anticipate that this simple, high-throughput, and versatile nanopore fabrication technique will find applications in other domains of the nanopore research field such as filtration, power generation and chemical sensing [4, 30, 31].

Results and discussion

Figure 1A outlines a schematic of the fabrication protocol for the production of a nanopore array in SiN. First, a layer a 100 nm thick layer of poly(methyl methacrylate) (PMMA-A3, 495K)

electron sensitive resist (MicroChem Corp) is spin-coated on top of the chip containing a freestanding SiN membrane. Subsequently, the layer is patterned by exposing the resist with a 100 keV electron bundle from the electron-beam pattern generator (EBPG5200, Raith), using one single shot of e-beam exposure per nanopore. Details about the fabrication of the support and E-beam patterning can be found in the Supporting Information (SI). After exposure, the PMMA is developed in a 1:3 mixture of methyl isobutyl ketone (MIBK) and isopropyl alcohol (IPA) for 1 min. Finally, the pattern is transferred into the SiN membrane by reactive ion etching with CHF_3 (100 sec, 50 W, 50 sccm of CHF_3, 2.5 sccm of O_2, 8.6 μbar, Leybold) and the resist is stripped in hot acetone (50°C) for 2 hours.

The fabrication of the graphene nanopore array (Fig. 1B) is analogous to the fabrication of the SiN nanopores. First, a layer of graphene (Graphenea, single layer CVD graphene on copper) is transferred onto a SiN membrane pre-patterned with square windows 1 μm in size, creating 1x1 μm freestanding areas of graphene (see SI). Then, a 150 nm thick layer of PMMA is spin-coated on top of the chip and the resist is exposed by a single shot from the electron beam. We note that thicker PMMA is used in the graphene nanopore arrays because the graphene requires an oxygen etch which also etches the PMMA mask substantially. After the development of the resist in 1:3 MIBK:IPA for one minute, the pattern is transferred into the graphene layer by reactive ion etching with oxygen (20 sec, 50 W, 20 sccm of O_2, 3.3 μbar, Leybold). The remaining resist is stripped for 20 min in hot m-xylene (85°C) and air-dried. To avoid collapsing the freestanding graphene layer, the sample is gently plunged vertically into the solution. After

20 mins, the sample is removed and placed at an angle (~20 degrees to the horizontal plane) to allow the remaining droplet of m-xylene to evaporate.

Figure 2 shows example TEM images of nanopore arrays fabricated in both SiN (Fig. 2A) and in freestanding graphene (Fig. 2B) using the protocol outlined above. The nanopores in these examples were 29 ± 3 nm and 38 ± 2 nm (average ± standard deviation) in diameter, for the SiN and graphene respectively. The nanopores produced are highly circular; The average ratio between their major and minor axis (major/minor) is 1.08±0.08 for the SiN arrays and 1.08±0.14 for the graphene nanopore arrays. We note that the graphene pores fabricated through this method seem to exhibit much less carbon deposition around the edges of the pore than conventionally drilled TEM graphene pores [32].

By adjusting the electron dose used in the patterning, we are able to vary the size of the nanopores formed, as shown in Fig. 3, where resulting diameter of the nanopore is plotted against the electron-beam dose used per shot of e-beam exposure, for both the SiN (Fig. 3A) and graphene nanopores (Fig. 3B). The smallest nanopore made was approximately 16±2 nm, both for SiN and graphene. Nanopores fabricated show similar variation in size (standard deviation is <10%) in both SiN and graphene. Because these values are similar and close to the size of the beamspot used (~15 nm), we speculate that the electron-beam spot size limits the resolution and hence it may be possible to fabricate smaller pores using a smaller spot size. By varying the electron-beam dose only, we obtained a range of nanopore sizes from 16 to >100 nm, though in

principle even bigger sized pores can be produced by rasterizing a larger area with multiple shots of e-beam exposure.

Interestingly, we find that the diameter of the resulting nanopore follows an empirical logarithmic relationship to the electron dose used for both SiN and graphene:

$$d = A \cdot log\,(D) + B \quad (1)$$

where d is the nanopore diameter, D is the total electron dose, and A and B are fit parameters. A least-squares fit of Eqn. 1 to the red data points is plotted as a solid blue line in Fig. 3 and shows good agreement with the data (SiN: $\chi^2_{red} = 2.8$, graphene: $\chi^2_{red} = 2.3$). The specific values of the fit parameters A and B are not universal and will depend on experimental factors, such as the membrane material, resist thickness and the electron accelerating voltage. For instance, a higher dose is needed to create the same size of nanopores in free standing graphene as compared to SiN. A different dependence results if patterning is performed on a thick substrate since electron backscatter from the substrate will be the dominant contribution to the exposure[28]. The agreement between the data and relationship is somewhat surprising as a more complex dependence is expected if one assumes that the nanopore size is merely set by the point spread function (PSF) of the electron beam[29]. This dependency can be modelled by assuming the resist only develops after receiving a local electron dose per unit area $\widetilde{D}$ larger than some threshold value of the dose D_T. Using a Gaussian PSF to describe the electron beam profile ($\widetilde{D}(r) \propto De^{-\gamma r^2}$, where r is the distance from the center of the electron beam, D is the total dose, and γ is a fit parameter) and setting $D_T = \widetilde{D}(d)$, a dependency of the diameter on the total dose can be

extracted. This dependency is plotted as a green line in Fig. 3 and does not explain the trend well. Only moderate agreement between data (SiN $\chi^2_{red} = 7.2$, graphene: $\chi^2_{red} = 10.8$) is obtained. Hence the phenomenological model in equation 1 should be used to determine the correct size of the nanopore from the dose.

One might wonder if the use of PMMA as a resist will set a maximum size for the nanopore size that can be fabricated, as it is known that PMMA will behave as a negative-tone resist at high doses[33] (>100fC). This is however not the case, as at high-dose exposure, the resist in the tail of the beam will still be exposed to a low dose. This leads to a donut-shaped cut in the resist after development which will create a hole in the membrane after pattern transfer by RIE. Moreover, standard resist patterning (rastering) can be used for nanopores larger than 50 nm in diameter or for large nanopores of different shapes.

To show that the SiN and graphene nanopores created using this method can be used for the detection of DNA, we performed double-stranded DNA (lambda-DNA, 48.5kbp) translocation experiments on these nanopores. A schematic of a typical nanopore experiment is shown in Fig. 4A, where DNA molecules added to the negatively-biased *cis* compartment of the flow cell are electrophoretically driven through the nanopore and detected by a change in ionic current through the pore. Fig. 4 shows examples of DNA translocations through a 18 nm graphene nanopore, fabricated using a dose of 88 fC, and a 25 nm SiN nanopore, fabricated using a dose of 15 fC. DNA translocation experiments were done in a PEEK (Polyether ether ketone) flow cell in 2M LiCl (buffered with 20mM Tris-Cl, 2mM EDTA, pH 8) and we used

Ag/AgCl electrodes and an Axopatch 200B amplifier (Molecular Devices) for current detection. To wet the graphene nanopore, we incubated the chip in the flow cell with a mixture of equal parts ethanol and water for 30 min.

Figure 4B shows the linear I-V curve of the SiN nanopore with a resistance of 4.5 MΩ. This compares well with the expected resistance of 3.9 MΩ for a 25 nm nanopore, calculated using a measured buffer conductivity of 13.8 nS/m and an effective membrane thickness of 6.7 nm. After adding lambda-DNA to the *cis* chamber at a concentration of 10 ng/μL, transient current blockades could be clearly discerned, as shown in the first panel of Fig. 4C. The translocations show excellent signal-to-noise characteristics, illustrated by the zooms in the right panel of Fig. 4C of two such DNA translocations, one molecule translocating in a linear fashion (right) and one in a folded conformation (left). The double-strand DNA conductance blockade of 1.8 nS (N = 580) matches the expected value of 1.8 nS well. The normalized current power spectral density can be found in the SI.

Fig. 4D shows example DNA translocations through a 18 nm graphene nanopore. The nanopore had a resistance of 4.9 MΩ, which agrees reasonably well with the expected 4.2 MΩ using an effective membrane thickness of 0.6 nm[34, 35]. We used a high driving voltage of 500 mV, to enhance the low capture rates often observed in bare graphene nanopores[36]. The current time trace shows considerable low-frequency current noise, similar to what was observed for TEM-drilled graphene nanopores[37] (see SI). Analysis[38] of all detected events at 500 mV (N = 59) show a blockade levels of ~1.0 nS. This is markedly lower than the theoretically expected

blockade of 5.6 nS from a dsDNA strand in a 18 nm graphene nanopore[39], but the discrepancy is consistent with previous work on TEM-drilled graphene nanopores which gave values of 1.5 nS for similar sized pores[32]. Graphene nanopores drilled using this RIE based method suffer from the same challenges as graphene nanopores drilled using TEM such as low fabrication yield. These challenges include limited statistics and current-signal resolving power caused by graphene-DNA interactions[40] and high 1/f noise[37]. Overall about 10% of the graphene devices showed successful DNA translocation events compared to over 50% in SiN devices. Fortunately, these issues can be mitigated by reducing the freestanding area and using a molecular coating of the graphene[36].

Summarizing, these nanopores created using EBL with RIE show sensing characteristics that are on par with their TEM-drilled counterparts.

Conclusions

In conclusion, we have developed a facile method for rapid, flexible, and large-scale nanopore manufacturing in freestanding SiN and graphene membranes using electron-beam lithography with reactive ion etching which are very commonly available fabrication techniques. As the nanopore is created in the final step of the fabrication, our approach is extremely versatile and can in principle by used on any substrate, in particular 2D materials that require a transfer step. By adjusting the electron-beam dose, the diameter of the nanopore can accurately be controlled with a high-level of uniformity and precision. Furthermore, we demonstrate that the nanopores

fabricated with this method show single-molecule sensing performances equivalent to their TEM drilled predecessors. The ease of the method allows for patterning large intact areas of freestanding 2D materials like graphene with a clearly defined array of nanopores. We expect that this technique will also find a range of applications beyond mere nanopore sensing, such as filtration with nano-sieves.

Acknowledgements

We like to thank Meng-Yue Wu for TEM imaging, Stephanie Heerema, Xin Shi, and Sergii Pud for the valuable discussions. This work was supported by the National Human Genome Research Institute of the National Institute of Health under Award Number R01-HG007406, ERC Advanced Grant SynDiv (No. 669598), and the Netherlands Organization of Scientific Research (NWO/OCW) as part of the Frontiers of Nanoscience Program.

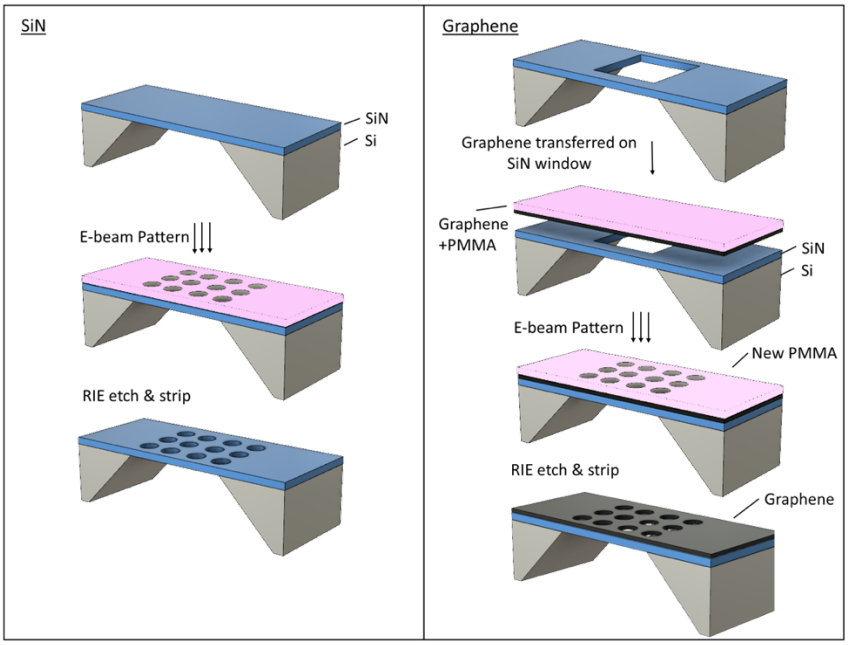

Figure 1. Schematic of EBL assisted RIE nanopore fabrication. A) Fabrication process on SiN membrane. A 100 nm thick layer of PMMA is spin-coated on a SiN membrane prior to e-beam patterning. The pattern is transferred into the SiN membrane by reactive ion etching in a CHF_3 plasma. Finally, the remaining resist is stripped in hot acetone (50°C) leaving a functional nanopore array. B) The same process on the graphene membrane. A graphene layer with a supporting PMMA layer is deposited on a pre-etched SiN window. The supporting layer of PMMA is stripped and a new 150 nm of PMMA is deposited prior to e-beam patterning. The pattern is transferred into the graphene membrane by reactive ion etching in an oxygen plasma. Finally, the remaining resist is stripped in m-xylene, leaving a functional nanopore array.

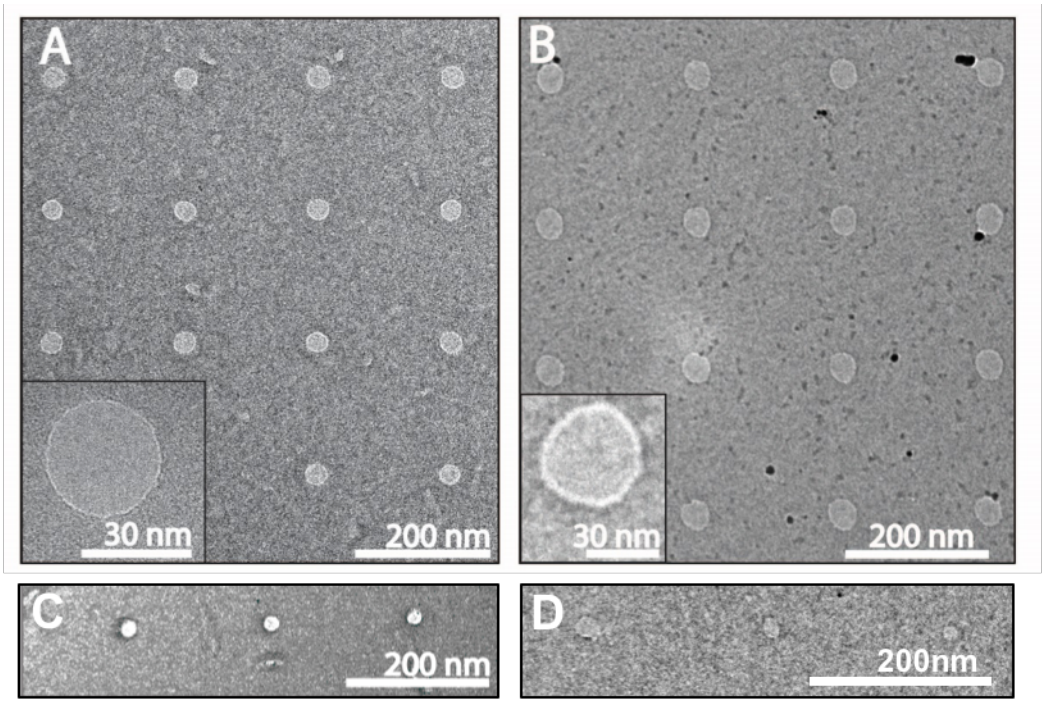

Figure 2. TEM image of nanopore arrays fabricated using RIE. A) Nanopore array fabricated in a SiN membrane. The array was fabricated using fabricated using a dose of 22 fC/shot, and the average pore diameter was 29±3 nm. B) Nanopore array fabricated in free-standing graphene. The array was fabricated using fabricated using a dose of 320 fC/shot, and the average pore diameter was 38±2 nm. The insets are zooms of a nanopore from each respective array, showing a circular nanopore. C) An array of 16±2 nm size pores in SiN. D) A dose test of nanopores on free-standing graphene. The nanopore diameters are, from left to right, 26nm, 19 nm, and 17 nm. More examples of nanopore arrays are attached in the Supporting Information.

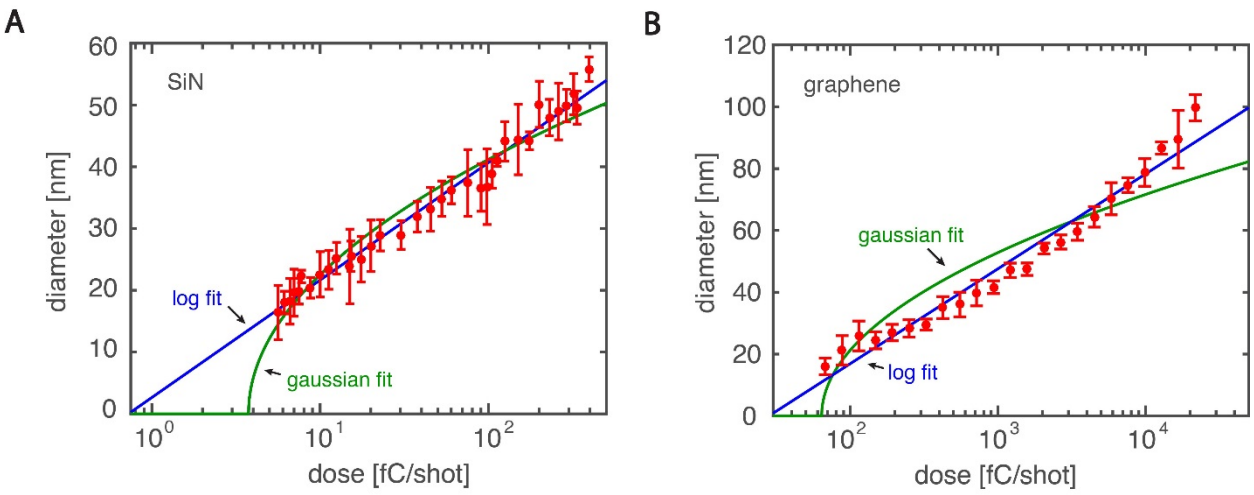

Figure 3. Single-shot nanopore diameter versus electron-beam dose. The solid blue line is an empirical logarithmic fit (A-SIN: $\chi^2_{red} = 2.8$, B- Graphene : $\chi^2_{red} = 2.3$), the green curve is a fit assuming a Gaussian dependence of dose on diameter (A-SiN: $\chi^2_{red} = 7.2$, B-Graphene: χ^2_{red} =10.8). Error bars are the standard deviation, χ^2_{red}values are calculated using the standard error of the mean for each datapoint.

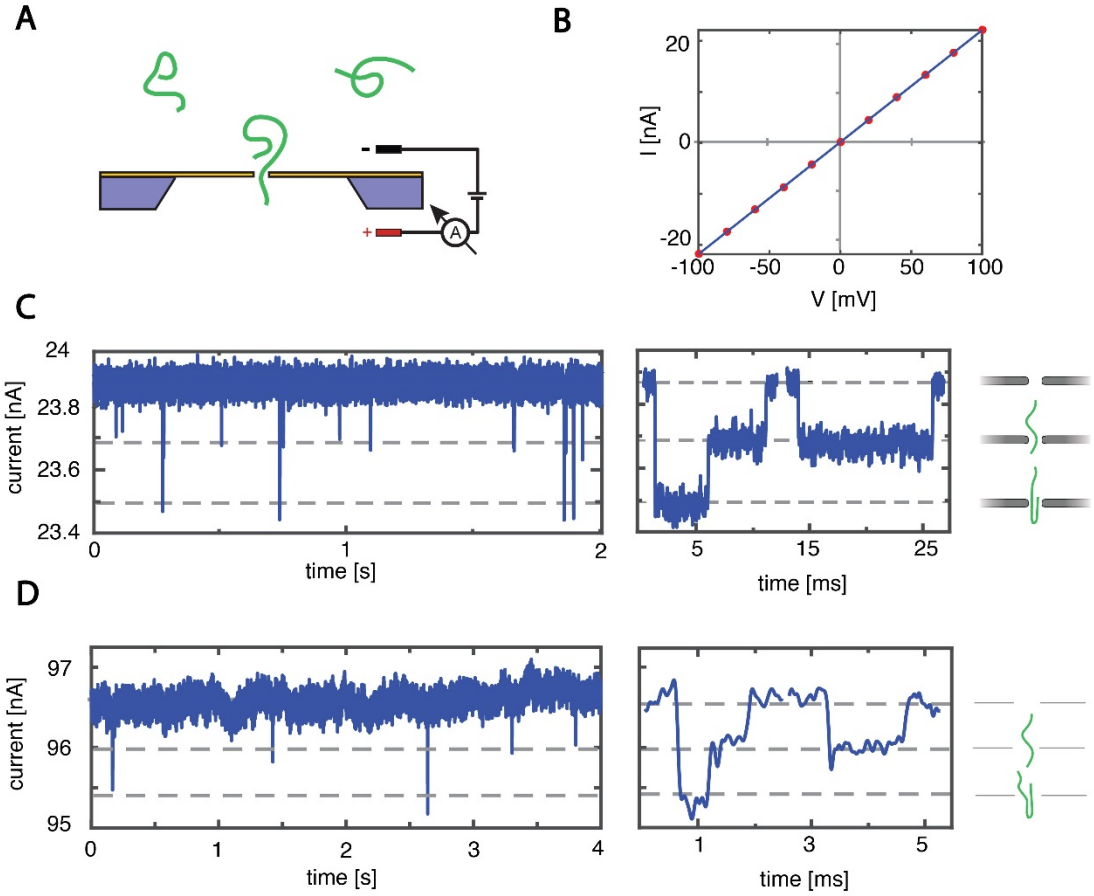

Figure 4. DNA translocations through RIE-fabricated SiN and graphene nanopores. (A) Schematic illustration of a DNA translocation experiment. (B) IV-curve of a 25 nm SiN nanopore with a resistance of 4.5 MΩ, with the corresponding linear fit. (C) Left: Current time trace through a SiN nanopore of 25 nm (4.5 MΩ). Data was taken at 100 mV in 2M LiCl and low-pass filtered at 10 kHz. Right: zooms of DNA translocations, showing a folded and a linear translocation. (D) Left: Current time trace through a graphene nanopore of 18 nm (4.0 MΩ). Data was taken at 500 mV in 2M LiCl and low-pass filtered at 5 kHz. The large driving voltage was used to enhance the DNA translocation rate. Right: zooms of DNA translocations, showing a folded and a linear translocation.

1. Arjmandi-Tash, H.; Belyaeva, L. A.; Schneider, G. F. *Chemical Society Reviews* **2016,** 45, (3), 476-493.
2. Miles, B. N.; Ivanov, A. P.; Wilson, K. A.; Doğan, F.; Japrung, D.; Edel, J. B. *Chemical Society Reviews* **2013,** 42, (1), 15-28.
3. Wanunu, M. *Physics of life reviews* **2012,** 9, (2), 125-158.
4. Feng, J.; Graf, M.; Liu, K.; Ovchinnikov, D.; Dumcenco, D.; Heiranian, M.; Nandigana, V.; Aluru, N. R.; Kis, A.; Radenovic, A. *Nature* **2016,** 536, (7615), 197-200.
5. Heerema, S. J.; Dekker, C. *Nature nanotechnology* **2016,** 11, (2), 127-136.
6. Chen, J.; Li, C.; Shi, G. *The journal of physical chemistry letters* **2013,** 4, (8), 1244-1253.
7. Jiang, D.-e.; Cooper, V. R.; Dai, S. *Nano letters* **2009,** 9, (12), 4019-4024.
8. Raillon, C.; Cousin, P.; Traversi, F.; Garcia-Cordero, E.; Hernandez, N.; Radenovic, A. *Nano letters* **2012,** 12, (EPFL-ARTICLE-176020), 1157-1164.
9. Goyal, G.; Lee, Y. B.; Darvish, A.; Ahn, C. W.; Kim, M. J. *Nanotechnology* **2016,** 27, (49), 495301.
10. Marshall, M. M.; Ruzicka, J.; Zahid, O. K.; Henrich, V. C.; Taylor, E. W.; Hall, A. R. *Langmuir* **2015,** 31, (15), 4582-4588.
11. Japrung, D.; Bahrami, A.; Nadzeyka, A.; Peto, L.; Bauerdick, S.; Edel, J. B.; Albrecht, T. **2014**.
12. Chen, K.; Juhasz, M.; Gularek, F.; Weinhold, E.; Tian, Y.; Keyser, U. F.; Bell, N. A. *Nano letters* **2017,** 17, (9), 5199-5205.
13. Sze, J. Y.; Ivanov, A. P.; Cass, A. E.; Edel, J. B. *Nature Communications* **2017,** 8, (1), 1552.
14. Kim, M. J.; Wanunu, M.; Bell, D. C.; Meller, A. *Advanced materials* **2006,** 18, (23), 3149-3153.
15. Deng, T.; Li, M.; Wang, Y.; Liu, Z. *Science bulletin* **2015,** 60, (3), 304-319.
16. Xu, Q.; Wu, M.-Y.; Schneider, G. F.; Houben, L.; Malladi, S. K.; Dekker, C.; Yucelen, E.; Dunin-Borkowski, R. E.; Zandbergen, H. W. *Acs Nano* **2013,** 7, (2), 1566-1572.
17. Yang, J.; Ferranti, D. C.; Stern, L. A.; Sanford, C. A.; Huang, J.; Ren, Z.; Qin, L.-C.; Hall, A. R. *Nanotechnology* **2011,** 22, (28), 285310.
18. Deng, Y.; Huang, Q.; Zhao, Y.; Zhou, D.; Ying, C.; Wang, D. *Nanotechnology* **2016,** 28, (4), 045302.
19. Kwok, H.; Briggs, K.; Tabard-Cossa, V. *PloS one* **2014,** 9, (3), e92880.
20. Kuan, A. T.; Lu, B.; Xie, P.; Szalay, T.; Golovchenko, J. A. *Applied physics letters* **2015,** 106, (20), 203109.
21. Zrehen, A.; Gilboa, T.; Meller, A. *Nanoscale* **2017,** 9, (42), 16437-16445.
22. Park, S. R.; Peng, H.; Ling, X. S. *Small* **2007,** 3, (1), 116-119.
23. Deng, T.; Chen, J.; Wu, C.; Liu, Z. *ECS journal of solid state science and technology* **2013,** 2, (11), P419-P422.
24. Yasuda, K.; Ghicov, A.; Nohira, T.; Kani, N.; Hagiwara, R.; Schmuki, P. *Electrochemical and Solid-State Letters* **2008,** 11, (9), C51-C54.

25. Han, A.; Creus, M.; Schürmann, G.; Linder, V.; Ward, T. R.; de Rooij, N. F.; Staufer, U. *Analytical chemistry* **2008,** 80, (12), 4651-4658.
26. Bai, J.; Wang, D.; Nam, S.-w.; Peng, H.; Bruce, R.; Gignac, L.; Brink, M.; Kratschmer, E.; Rossnagel, S.; Waggoner, P. *Nanoscale* **2014,** 6, (15), 8900-8906.
27. Ahmadi, A. G.; Nair, S. *Microelectronic Engineering* **2013,** 112, 149-156.
28. Wei, R.; Pedone, D.; Zürner, A.; Döblinger, M.; Rant, U. *Small* **2010,** 6, (13), 1406-1414.
29. Adesida, I.; Everhart, T.; Shimizu, R. *Journal of Vacuum Science and Technology* **1979,** 16, (6), 1743-1748.
30. Aghigh, A.; Alizadeh, V.; Wong, H. Y.; Islam, M. S.; Amin, N.; Zaman, M. *Desalination* **2015,** 365, 389-397.
31. Howorka, S.; Siwy, Z. *Chemical Society Reviews* **2009,** 38, (8), 2360-2384.
32. Schneider, G. F.; Kowalczyk, S. W.; Calado, V. E.; Pandraud, G.; Zandbergen, H. W.; Vandersypen, L. M.; Dekker, C. *Nano letters* **2010,** 10, (8), 3163-3167.
33. Duan, H.; Winston, D.; Yang, J. K.; Cord, B. M.; Manfrinato, V. R.; Berggren, K. K. *Journal of Vacuum Science & Technology B, Nanotechnology and Microelectronics: Materials, Processing, Measurement, and Phenomena* **2010,** 28, (6), C6C58-C6C62.
34. Heerema, S. J.; Schneider, G. F.; Rozemuller, M.; Vicarelli, L.; Zandbergen, H. W.; Dekker, C. *Nanotechnology* **2015,** 26, (7), 074001.
35. Rollings, R. C.; Kuan, A. T.; Golovchenko, J. A. *Nature communications* **2016,** 7.
36. Schneider, G. F.; Xu, Q.; Luik, S.; Hage, S.; Spoor, J. N.; Malladi, S.; Zandbergen, H.; Dekker, C. *Nature communications* **2013,** 4, 2619.
37. Heerema, S.; Schneider, G.; Rozemuller, M.; Vicarelli, L.; Zandbergen, H.; Dekker, C. *Nanotechnology* **2015,** 26, (7), 074001.
38. Plesa, C.; Dekker, C. *Nanotechnology* **2015,** 26, (8), 084003.
39. Carlsen, A. T.; Zahid, O. K.; Ruzicka, J.; Taylor, E. W.; Hall, A. R. *Acs Nano* **2014,** 8, (5), 4754-4760.
40. Kabiri, Y.; Ananth, A. N.; van der Torre, J.; Katan, A.; Hong, J. Y.; Malladi, S.; Kong, J.; Zandbergen, H.; Dekker, C. *Small* **2017**.